Mössbauer spectroscopy as a nuclear probe for solid state transuranium chemistry

J. Jové, L. He*, J. Proust and M. Pagès

Institut Curie, Section de Physique et Chimie, Physicochimie des Eléments Transuraniens (UA 448 CNRS), 11 rue Pierre et Marie Curie, 75231 Paris Cedex 05 (France)

P. Pyykkö

University of Helsinki, Department of Chemistry, Et. Hesperiankatu 4, 00100 Helsinki (Finland)

Abstract

Some applications of Mössbauer spectroscopy to the study of insulating neptunium compounds are reported here. After a short introduction to hyperfine parameters useful for the chemist, some correlations between isomer shift, electric field gradient and neptunium bonding or crystallographic structure are discussed. A review of selected examples of recent studies regarding local order and isomer shift of neptunium in crystallized or amorphous compounds for each charge state of Np(III–VII) follows. Finally, an attempt is made to correlate the electronic structure and bonding in insulating neptunium compounds to isomer shift and electric field gradient with calculations using the relativistic extended Hückel method.

1. Introduction

The first elements in the series of 5f elements, thorium to americium, have properties which are intermediary between those of the 3d and 4f elements. In this series, the relativistic effects are maximal. A broader extension of the 5f orbitals (in comparison with the 4f ones) provides them with properties common to those of the 3d and 4f elements, as well as their own specific properties. The 5f electrons participate in bonding and numerous charge states exist: five for neptunium, from III to VII, all stable in the solid state.

The interest in Mössbauer spectrometry (nuclear gamma resonance) is due essentially to the fact that the "Mössbauer" nucleus behaves like a very sensitive local probe which can provide information on the resonant nucleus and its environment. This method is particularly well adapted to the study

---

*Present address: Iowa State University, Ames IA 50010, U.S.A.

of the actinides. It is not destructive and requires relatively small quantities of samples (≈ 100 mg). It can be applied to polycrystalline and amorphous compounds and is selective with regard to impurities.

Mössbauer spectrometry can be used for [231]Pa, but the latter has only one charge state, V. For [238]U and [240]Pu, owing to problems of source, the insensitivity of the isomer shifts to the charge states and the width of the resonance line, little information can be obtained. [243]Am can be studied, but this isotope is rare and the short half-life of the source ($T = 5$ h) makes it necessary to work near a nuclear reactor. The amounts of available [246]Cm (parent [250]Cf) are inconsequential.

Fortunately, [237]Np, which is well represented among the light actinides, is one of the best Mössbauer nuclei in the periodic table. The high transition energy (59.6 keV for the transition $\frac{5}{2}^- \to \frac{5}{2}^+$ of [237]Np) permits the use of perfectly tight double aluminium containers.

Mössbauer spectrometry of neptunium has been extensively described in numerous articles and reviews [1-4]. In this work, two hyperfine parameters, useful to the chemist, will be briefly examined, and, using some carefully chosen examples, the advantages of Mössbauer spectrometry in the study of neptunium–ligand bonding and the neptunium environment of salt compounds will be illustrated (Table 1). The semi- and organo-metallic compounds which have a different behaviour were described elsewhere [1, 4-6].

Three principal effects are observed:

(1) The monopolar electric interaction derives from the coupling between the charge distribution of the protons in the nucleus and that of the electrons penetrating the nuclear volume. It leads to the isomer shift S. The electronic charge density inside the nuclear volume $\rho_e(0)$ results from the direct contribution of the s electrons (and relativistic $p_{1/2}$); the p, d or f electrons interact indirectly via a screening effect.

For [237]Np: S (mm s^{-1}) $= 9.5 \, \rho_e(0) \Delta \langle r^2 \rangle$, with $\rho_e(0)$ in a_0^{-3}, and $\Delta \langle r^2 \rangle$ in fm^2; the difference in mean square nuclear charge radius between ground state and excited state has a negative sign (-27×10^{-3} fm^2). $\rho_e(0)$ is sensitive to any modification in the valence electrons (Np: $7s^2$, $5f^4$, $6p^6$, $6d^1$). The isomer shift provides information on the charge state, the number of sites containing the resonant atom and the distribution of the sites, the nature of the neptunium–ligand bonding, the number and distance of the nearest neighbours and on the electronic populations. In the absence of other effects, the Mössbauer spectrum is a single lorentzian line (Fig. 4(a)). $\rho_e(0)$ decreases with the number of 5f electrons, while S becomes more positive. *Ab initio* molecular orbital calculations in neptunium compounds are still not possible. The theoretical calculation of $\rho_e(0)$ has been performed only for the free $5f^n$ ion configurations [13a, 29, 30]. These calculations, therefore, do not take into account the solid environment and the recently discovered contribution of the 6p electrons to bonding [31, 32]. The considerable amount of information which is already available does, however, allow correlation between isomer shift with the electronic structure using semiempirical methods [19, 33].

TABLE 1

Hyperfine parameters of neptunium ionocovalent compounds obtained at $T = 4.2$ K.

Compound	CN	$e^2 qQ$ (mm s^{-1})	η	Ref
Ba_2NaNpO_6	6	0	0	8
Na_5NpO_6		24	1	8
K_3NpO_5		0	0	8
Rb_3NpO_5		90	0.13	9
Cs_3NpO_5		81	0.15	12, 9
Frozen solution		88	0.56	10, 11
$KNpO_4$	6	145	0	12
$CsNpO_4$		138	0.15	12, 9
Sr_3NpO_6		0	0	8
Ba_3NpO_6	6	0	0	16
$Ba_2MNpO_6^a$ (M=Fe, Co, Ni, Zn)		0	0	14, 15
$K_2NpO_4^a$	6	88	0	16
$BaNpO_4^a$		102	0.37	17, 18
$(NH_4)_3NpO_2F_5$	7	176	0.15	19
$Tl_2(NpO_2)_2V_2O_8$		168	0.30	20
$BaMnNpO_6^a$	6	0	0	14
NpO_2CO_3	8	224	0.21	21
NpO_2F_2		220	0	19
$Na_4(NpO_2)_2C_{12}O_{12}$		105	0	22
$(NpO_2)_2SO_4 2H_2O$	7	82	0	23
Frozen solution		106	0	10
$NH_4NpO_2F_2$	8	84	0	19
$KNpO_2CO_3$	8	100	0	25
$BaNpO_3^a$	6	19	0	24
NpO_2^a	8	0	0	26
$CaNp(PO_4)_2$	9	44	0	27
$Np_{0.5}^{III}Eu_{0.5}F_3$	9	17	1	19
$ZrNp_{0.27}^{III}Np_{0.73}F_7O_{0.365}$ (glass)	8–9	0	0	28

S (mm s^{-1})
Ref. NpAl$_2$ [7]

-80, -70, -60, -50, -40, -30, -20, -10, 0

NpF$_6$ [13], NpF$_5$ [13], NpF$_4$ [19], NpF$_3$ [19], 40

Np^{VII}, Np^{VI}, Np^{V}, Np^{IV}, Np^{III}

^{a}Values obtained at $T = 77$ K: $S =$ isomer shift; quadrupole splitting 1 mm s$^{-1} = 48.02$, $M_c = 2 \times 10^{-7}$ eV, $Q_{Np} = 4.1$ b.k.; $\eta =$ asymmetry parameter. The error on S is 2.5%, on e^2qQ is 1%, and on η is 10%. Mössbauer spectra are fitted using the MÖSFUN program [48].

(2) The e^2qQ quadrupolar electric interaction is produced by the coupling between the quadrupolar moment Q of the nucleus and the non-spherical distribution of the electrical charges (ionic charge on the lattice and contribution of the 5f or 6p electrons) which induces an electrical field gradient (EFG) at the site of the resonant nucleus, $\text{EFG} = eq = V_{zz}$. The quadrupole splitting e^2qQ provides information on the symmetry of the site (coordination polyhedron) and on the 5f and 6p contributions.

Three cases may be noted:

(i) EFG with axial symmetry: the spectrum shows five lines and is symmetric with respect to the central line. The spectrum is more or less resolved depending on the value of eq (Fig. 4(b), (c)).

(ii) Non-axially symmetric EFG: here a parameter of asymmetry must be brought in ($\eta = (V_{xx} - V_{yy})/V_{zz}$, $0 < \eta < 1$). The spectra remain symmetric with respect to the central line.

(iii) When $\eta = 1$ (if one forgets the weak forbidden transitions) the spectrum has three lines (Fig. 7(c)).

(3) Dipolar magnetic interaction has its origin in the coupling of a magnetic dipole moment, Φ_I, of a spin I nuclear level, with the magnetic field B_{eff} at the nucleus site. The spectrum, which is symmetrical for pure magnetic splitting, has 16 lines. In the case of non-collinear magnetic and quadrupolar interactions, the spectrum becomes more complex. Relaxation phenomena produced by dynamic interactions (spin fluctuations) lead to more or less well resolved spectra, according to the relaxation time. When the relaxation time is very large, if compared with the Larmor precession period, a static hyperfine magnetic field is observed. In a more detailed discussion one would have to distinguish relaxation processes in a paramagnet or in an ordered magnet.

Due to the relativistic effects, the Mössbauer parameters are very extended for neptunium: for Np(VII) to Np(III) S increases from -80 to $+40$ mm s^{-1}, while e^2qQ can reach 230 mm s^{-1} (Table 1). Even so, striking differences between the various charge states are noted. All the neptunium compounds are distributed on the isomeric shift scale as a function of the neptunium charge state. Although maximal for Np(VI), S variations are still large for Np(V) and Np(VII); however they become weak for Np(IV), and all the Np(III) compounds have the same isomer shift within the limit of experimental error (Table 1).

2. Correlation between S and $\langle d_{\text{Np-L}} \rangle$ and between S and e^2qQ for neptunium(VI) compounds

Various oxides, fluorides, oxyfluorides and polycarboxylic complexes of neptunium, from III to VII oxidation states have been studied for different neptunium environments (Table 1).

Correlations between the isomer shift and the mean neptunium–ligand distance, as well as between S and e^2qQ have been observed for Np(VI)

compounds containing the neptunyl ion NpO_2^{2+} [1]. These correlations have been completed and extended to other Np(VI) compounds.

One of the essential characteristics of the 5f elements is the formation of the AO_2^{n+} actinyl ion ($A \equiv U$, Np, Pu and Am), with two O1 atoms for the nearest neighbours and four, five or six ligands L_{II} in the equatorial plane. The neptunyl group, which is linear in most cases, dominates the neptunium–ligand bonding, usually providing axial symmetry. For NpO_2^{2+}, 12 valence electrons fill all the bonding orbitals, ensuring very strong covalent bonding (UO_2^{2+} structure to which a 5f electron has just been added in a non-bonding orbital). It should be noted that for two compounds having the same coordination (e.g. VI), the presence of the neptunyl group has little influence on the isomer shift but induces a strong electrical field gradient: S varies between Ba_2CoNpO_6 [15], non-neptunyl NpO_6^{6-} group and β-Na_2NpO_4 [34] neptunyl NpO_2^{2+} group, from -59.3 to -56.2 (3) mm s^{-1}, while e^2qQ increases from 0 to 102 mm s^{-1} (Table 1).

The variation in isomer shift as a function of $\langle d_{Np-L} \rangle$ is linear (Fig. 1). A more straightforward correlation is obtained if oxides and fluorides are considered separately. It is shown that all these compounds are located in three areas (Fig. 1) which are well defined according to their coordination (VI, VII or VIII).
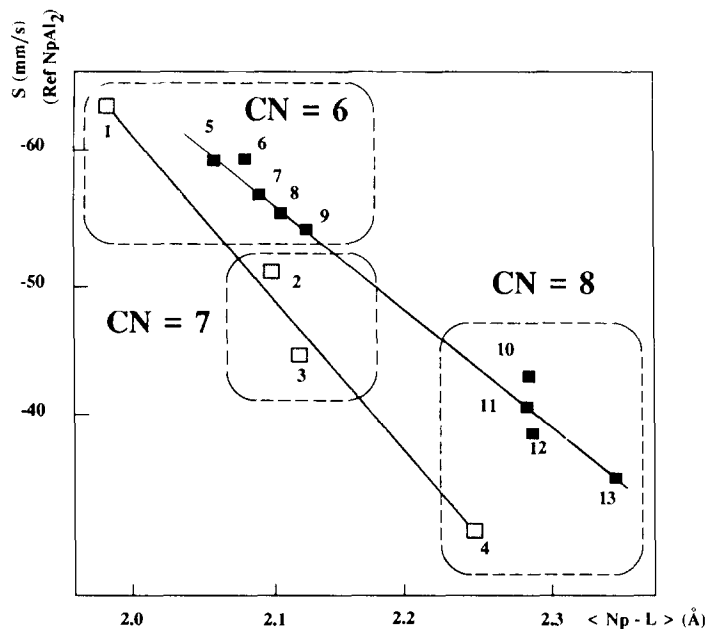

Fig. 1. Isomer shift for hexavalent neptunium compounds vs. the mean $\langle Np-L \rangle$ bond length. The $\langle Np-L \rangle$ distance may be deduced from isomorphous uranium compounds using the relation: $\Delta(R_U^{VI}-R_{Np}^{VI}) = 0.1$ Å, where R is the ionic radius of the hexacoordinated ion. CN = coordination number. $1 = NpF_6$, $2 = K_3NpO_2F_5$, $3 = (NH_4)_3NpO_2F_5$, $4 = NpO_2F_2$, $5 = Ba_2CoNpO_6$, $6 = Li_4NpO_5$, $7 = K_2NpO_4$, $8 = \beta$-Na_2NpO_4, $9 = BaNpO_4$, $10 = NpO_2(NO_3)_2 \cdot 6H_2O$, $11 = NaNpO_2(C_2H_3O_2)$, $12 = RbNpO_2(NO_3)_3 \cdot 6H_2O$, $13 = NpO_2CO_3$; ■ oxides, ▨ fluorides.

There is also a correlation between e^2qQ and S (Fig. 2): all the Np(VI) compounds containing the neptunyl group are distributed in three well-defined regions. The non-neptunyl compounds are located separately, to the left (Fig. 2). It is noted that the nitrate $NpO_2(NO_3)_2 \cdot xH_2O$ [24], in which the presence of the neptunyl ion is suspected, is not in the corresponding zone and that the local environment of neptunium must thus be different from the one proposed.

Correlations also exist for the other neptunium charge states. There is a linear variation of e^2qQ as a function of S for the Np(VII) compounds, as well as of S as a function of the electronegativity of the ligand in the tetravalent halides [36].

These correlations permit the study of compounds whose structures are not known, $i.e.$ polycrystalline samples, in the absence of single-crystal data, and amorphous compounds. Besides optical spectroscopy, EXAFS and neutron diffraction, Mössbauer spectrometry is one of the few methods available to provide information on the local environment for such compounds. Let us take the case of neptunium compounds having analogous chemical formulae with corresponding uranium compounds whose structure is well established: the determination of the local order can lead to a conclusion (or not) regarding structural identity. Moreover, in some cases, Mössbauer spectrometry is able to provide complementary information on the corresponding uranium compound and more particularly on the presence of different charge states.
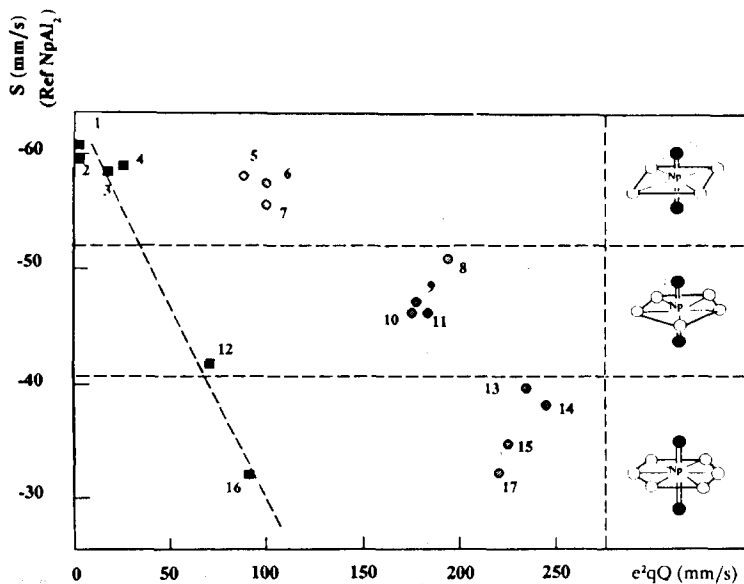

Fig. 2. Isomer shift $vs.$ electric field gradient: ⊘ neptunyl compounds; ■ non neptunyl compounds.
$1 = NpF_6$, $2 = Ba_2CoNpO_6$, $3 = Ba_2CuNpO_6$, $4 = Li_4NpO_5$, $5 = K_2NpO_4$, $6 = \beta\text{-}Na_2NpO_4$, $7 = BaNpO_4$, $8 = K_3NpO_2F_5$, $9 = (NH_4)_3NpO_2F_5$, $10 = K_2(NpO_2)_2V_2O_8$, $11 = Tl_2(NpO_2)_2V_2O_8$, $12 = NpO_2(NO_3)_2 \cdot 6H_2O$, $13 = NaNpO_2(CH_3CO_2)_3$, $14 = RbNpO_2(NO_3)_3 \cdot 6H_2O$, $15 = NpO_2CO_3$, $16 = CaNpO_4$, $17 = NpO_2F_2$.

3. Relationship between the Mössbauer parameters and local order

3.1. Neptunium(VI) compounds

The interest in these compounds is due to the fact that they exhibit a wide structural variety, for instance, perovskite-like structure and their derivatives, NaCl type, or distorted $R\bar{3}m$ and fluorite type [37]. Numerous coordination polyhedra, octahedral, pentagonal or hexagonal bipyramidal, deformed or not, are found.

3.1.1. Hexacoordinated Neptunium(VI)

3.1.1.1. Perovskite-type compounds: double perovskite. All compounds in the Ba_2MNpO_6 series, with M ≡ Fe, Co, Ni, Cu and Zn, are double ordered perovskites [15] (space group $Fm3m$) (Fig. 3(b)), with the exception of iron, which has a simple perovskite-type structure, $Pm3m$ (Fig. 3(a)). The coordination polyhedron is always a regular or distorted octahedron. The actinide and 3d element alternatively occupy the octahedral site. The octahedra form tridimensional chains connected by their six corners. The Mössbauer spectrum consists of a single line (Fig. 4(a)) with $S = -59.0$ (5) mm s^{-1} which is independent of M for all the compounds in the series. A charge distribution of spherical symmetry (O_h) corresponds to the regular octahedron (O_h), thus, $e^2qQ \approx 0$. This is the case for all the compounds in the series, with the exception of copper, for which $e^2qQ = 24$ mm s^{-1}. This is due to the Jahn–Teller effect of the copper which induces a deformation in the octahedron.

Ba_3NpO_6 and Sr_3NpO_6 (type Ba_2CoNpO_6) Mössbauer spectra are also perovskite type, their structure being unknown [38]. Barium and strontium occupy the barium site, as well as one-half of the octahedron sites: $Ba(Ba_{0.5}Np_{0.5})O_3$ (Fig. 3(b)).

3.1.1.2. Perovskite-type compounds: bidimensional perovskites of the K_2NiF_4 type. Quadratic, K_2NpO_4, $I4/mmm$ space group [16], orthorhombic $BaNpO_4$ (*Pbcm*), and β-Na_2NpO_4, bidimensional perovskite type, have a layered structure like La_2CuO_4.

The structural study carried out on the isostructural uranium compound has shown that β-Na_2NpO_4 crystallizes in the orthorhombic system (*Fmmm*). In this type of compound, the hexavalent actinide is located at the centre of a flattened octahedron (NpO_2^{2+} group). The octahedra, connected by four corners, form layers which are parallel to the xy plane. In K_2NpO_4, the layers are parallel (Fig. 3(c)). In $BaNpO_4$, the octahedra are bent as indicated in Fig. 5(c); the deformation of the octahedron leads to the existence of an asymmetry parameter $\eta = 0.37$ [17]. In β-Na_2NpO_4, the presence of four possible orientations of the flattened octahedrons in relation to the $P2_1/b$ crystal cell (Fig. 5(a)) is revealed. The angle ϑ between the xy plane and the $c4$ axis of the octahedron is equal to $34.83°$ (Fig. 5(d)). This structure should correspond to the delocalization of the oxygen atoms of the plane of octahedra and produce a broadening of the Mössbauer spectrum. The
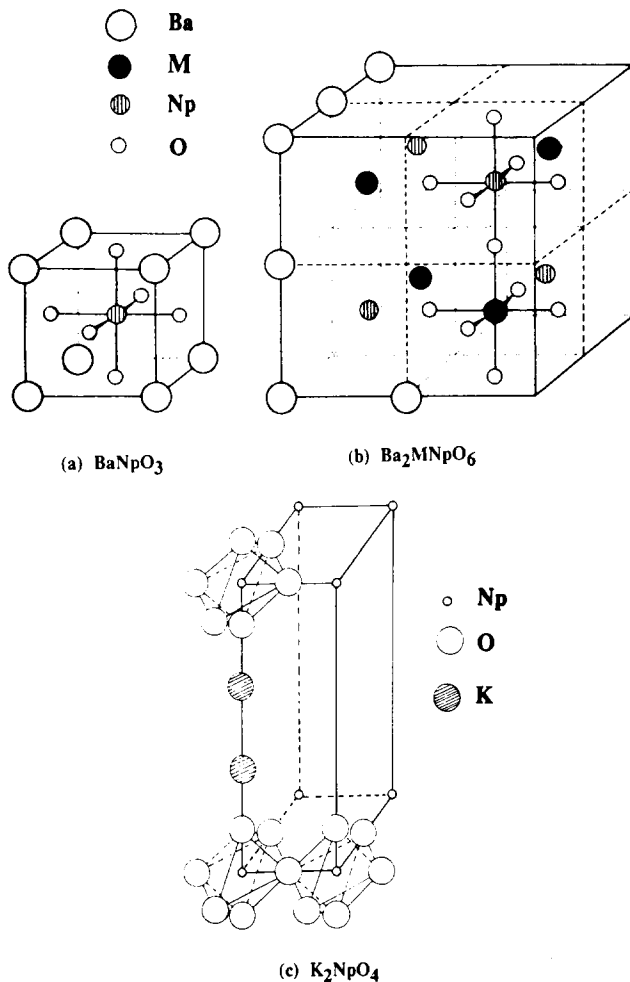
(a) BaNpO$_3$

(b) Ba$_2$MNpO$_6$

(c) K$_2$NpO$_4$

Fig. 3. Perovskite structure. (a) Simple perovskite, shown as idealized cubic BaNpO$_3$. (b) Ordered perovskite Ba$_2$MNpO$_6$ (BaM$_{0.5}$An$_{0.5}$O$_3$). (c) K$_2$NpO$_4$: K$_2$NiF$_4$ structure type, with neptunyl NpO$_2^{2+}$ ion.

Mössbauer spectrum of β-Na$_2$NpO$_4$ at 77 K shows a pure quadrupolar pattern with five narrow lines revealing a single crystallographic site for neptunium (Fig. 4(c)).

3.1.1.3. Perovskite-type compounds: neptunium perovskite of YBa$_2$CuO$_{7-x}$ type. The new high-temperature ($T_c = 20$–100 K) superconductors are oxide-based ceramics (from rare earths, alkaline earths, bismuth and copper, for the most part). The element responsible for superconductivity is copper. Their crystalline structures are relatively well known and are shared by three main families, all of which are derivatives of perovskite. An attempt has been made to substitute neptunium [40] (whether or not the charges
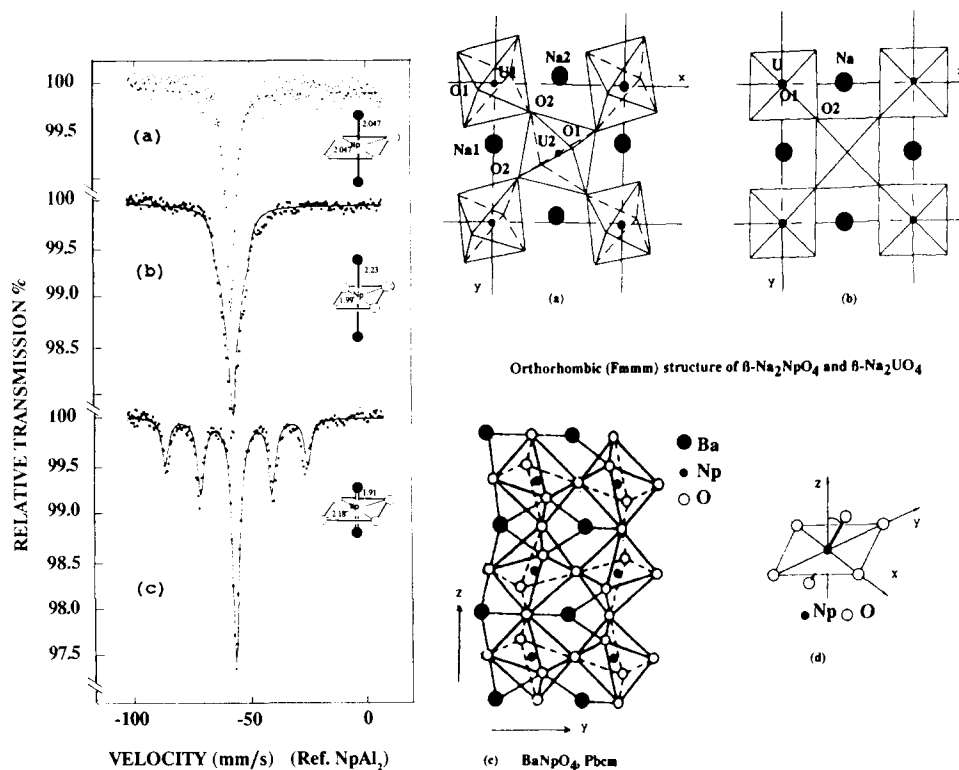
Fig. 4. Mössbauer spectra of hexacoordinated hexavalent neptunium compounds at 77 K. (a) Ba_2ZnNpO_6, double perovskite, with Np^{VI} ion in the centre of a regular octahedron. (b) Li_4NpO_5 with Np^{VI} in an elongated octahedron. (c) β-Na_2NpO_4 bidimensional perovskite, with NpO_2^{2+}, in a flattened octahedron.

Fig. 5. Perovskite structure. (a) Projection of a $P2l/b$ domain β-Na_2NpO_4 and β-Na_2UO_4 perovskite. (b) Projection between $Z=0$ and $Z=\frac{1}{4}$ of the idealized β-Na_2UO_4 structure. (c) Projection of the AnO_6 octahedra in the plane (y, z) for $BaNpO_4$. (d) Angle between the neptunyl ion (EFG axis) and the z-axis in β-Na_2UO_4.

are compensated) at the site of the rare earth in the high-temperature superconductor $YBa_2Cu_3O_{7-x}$.

Various compounds were studied, and, more particularly $Y_{0.9}Np_{0.1}Ba_2Cu_3O_{7-x}$ and $Ca_{0.5}Np_{0.5}Ba_2Cu_3O_{7-x}$. The pure orthorhombic phase $Y_{0.9}Np_{0.1}Ba_2Cu_3O_{7-x}$ was prepared. However, annealing at 900 °C under an oxygen flow led to a compound isostructural with Ba_2CuNpO_6 (Fig. 3(b)), a double perovskite. The X-ray diffraction spectrum of $Ca_{0.5}Np_{0.5}Ba_2Cu_3O_{7-x}$ annealed in air does not allow its structure to be determined. Mössbauer spectrometry (same spectrum as that of Ba_2CoNpO_6, $e^2qQ=0$ and $S=-60$ mm s^{-1}) reveals the occurrence of Np(VI) located at the centre of a regular octahedron. None of the phases studied was superconductive, probably because of the high neptunium charge state.

3.1.1.4. Perovskite-type compounds: KUO₃ perovskite-like compounds.
3.1.1.4. Perovskite-type compounds: KUO_3 perovskite-like compounds.
In the oxygenated neptunium–potassium system, for phases rich in potassium, in addition to tetragonal K_2NpO_4, compounds of KUO_3 perovskite type were obtained [41]. Crystal chemistry suggests the charge state V for the actinide, based on the isotypy. Mössbauer spectrometry shows that in this compound neptunium, as in K_2NpO_4, is hexavalent, with an NpO_2^{2+} ion at the centre of a flattened octahedron (same spectrum as in Fig. 4(c)). A uranium compound having a formula close to that of KUO_3 was thus synthesized: $K_9U_6O_{22.5}$. A structural study revealed the same local order as Mössbauer spectrometry. Moreover, it showed that it is perovskite like, obtained by doubling the KUO_3 cell in the three directions. Vacancies are found on O1, an unusual location, and on K2 ($K_8K\blacksquare Np_6O_{22.5}\blacksquare$). A fraction of the potassium atoms take the place of neptunium (K2); K^+, being larger than the actinide, requires two oxygen atoms closer to neptunium, forming NpO_2^{2+}.

3.1.1.5. Perovskite-type compounds: monoclinic perovskite. As shown, $K_9U_6O_{22.5}$ contains vacancies. It is interesting to prepare a perovskite without vacancies: $Na_8Ca_2A_6O_{24}$, for example. In fact $Na_8Np_{3.7}Ca_{3.11}O_{17.35}$ also having cationic vacancies at the actinide and the oxygen sites was obtained: $Na_8(Np^V_{0.89}Ca_{3.11})(Np^{VI}Np^V\blacksquare_{1.19})O_{17.35}\blacksquare_{6.65}$ [42].

The distribution of the uranium, calcium atoms and cationic vacancies (on U2) (Fig. 6(a)) was very close to that observed for double perovskites $Ba_2M^{II}NpO_6$. A single crystal of the uranium compound has been studied. Mössbauer spectrometry (Fig. 6(b)) revealed the presence of two charge states, Np^V and Np^{VI} ions ($S = -312.2$ and -55.9 mm s^{-1} respectively) in VI coordination. The line broadening should be due to the presence of vacancies. The high value obtained for e^2qQ (108 and 89 mm s^{-1}) and for η (0.75 and 1) respectively, correspond to very irregular octahedra. In agreement with the structural study, these values exclude the presence of
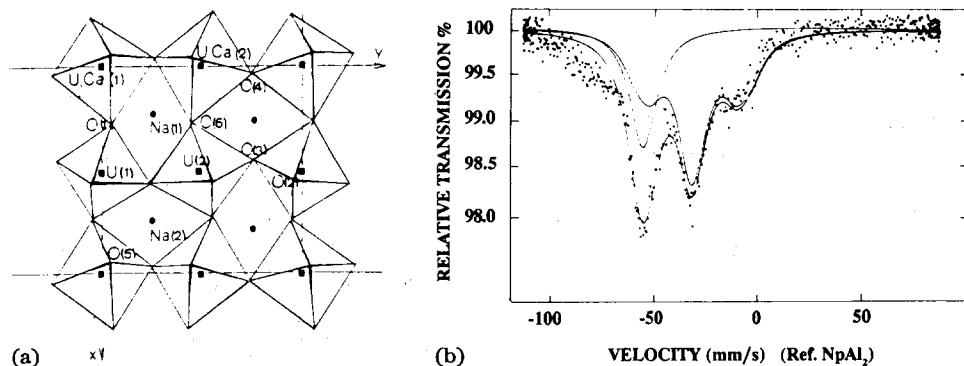

Fig. 6. Monoclinic perovskite. (a) Projection of AnO_6 octahedra along the z-axis. (b) ^{237}Np Mössbauer spectrum of $Na_8Np_2Np_{0.81}(Np_{0.89}Ca_{3.11})O_{17.35}$ at $T = 77$ K with the Np^V and Np^{VI} subspectra.

the actinyl ion in these compounds. This situation does not occur very frequently in neptunium compounds.

3.1.1.6. Li₄NpO₅. In tetragonal Li_4NpO_5, space group $I4/m$, the Np(VI) ion is at the centre of an elongated octahedron forming the NpO_4^{2-} "anti-neptunyl" group (Fig. 4(b)), with four oxygen atoms as nearest neighbours in the equatorial plane and two further oxygen atoms. The octahedra connected by two corners form linear chains parallel to the c axis. The e^2qQ of 18 mm s^{-1} is much weaker than that induced by the neptunyl group in an octahedron: 80 to 100 mm s^{-1} [19].

3.1.2. Neptunium(VI) in VII coordination

These compounds clearly illustrate the influence of the addition of a supplementary ligand to the neptunyl group. In $M_2(NpO_2)_2V_2O_8$ with M = K, Rb and Tl [20], (Fig. 7(a)), and $(NH_4)_3NpO_2F_2$ [19], the Np(VI) ion, with five fluorine atoms in the equatorial plane, is in coordination VII, at the

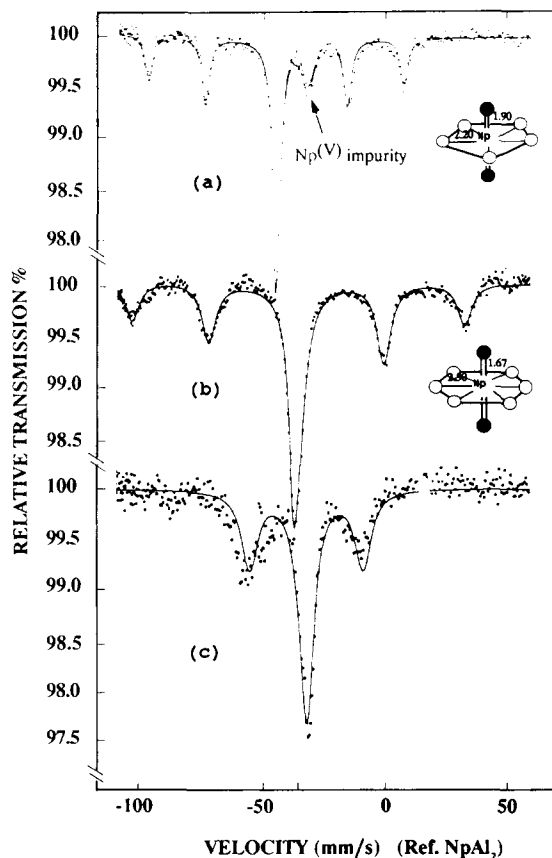Fig. 7. Pure quadrupole splitting in Mössbauer spectra at 4.2 K for: (a) $Rb_2(NpO_2)_2V_2O_8$, Np^{VI} ion at the centre of a pentagonal bipyramid; the additional line (↑) is due to the presence of an impurity. (b) NpO_2CO_3, with Np^{VI} in a hexagonal bipyramid. (c) $CaNpO_4$, $\eta = 1$.

centre of a pentagonal bipyramid. This increase of coordination from VI to VII produces a more positive isomer shift of 10 mm s^{-1}, while e^2qQ increases from 100 to 200 mm s^{-1}.

3.1.3. Neptunium(VI) in VIII coordination

In NpO_2CO_3 [21], (Fig. 7(b)), and NpO_2F_2 [19], the NpO_2^{2+} ion is surrounded by six ligands and is at the centre of a hexagonal bipyramid; the increase of S is so large that these compounds are located in the area of Np(V) on the isomer shift scale. This result reveals the possibility of overlapping among the neptunium charge states: two neptunium compounds can, with different electronic structures, have the same isomer shift. This points to the importance of hybridization of the orbitals in these compounds.

3.1.4. $R\bar{3}m$-like compounds

The U(VI) ion in $CaUO_4$ is surrounded by eight oxygen atoms, two of which, the O_I atoms, are closer (UO_2^{2+} ion) forming a hexagonal bipyramid. Distances between O_{II} atoms, $d(O_{II}-O_{II}) = 2.46$ Å, are unusually short [43]. In $Na_2U_2O_7$ [34] and $K_2U_2O_7$ [44], with the same structural type, the U_I and O_{II} atoms are delocalized and vacancies are found on O_I and O_{II}. The X-ray diffraction patterns of $Na_2Np_2O_7$, $K_2Np_2O_7$ and $CaNpO_4$ [43] are similar to that of $CaUO_4$, but the doubling of one line indicates a symmetry which is lower than $R\bar{3}m$. Mössbauer spectra reveal various environments in the corresponding neptunium compounds:

The $CaNpO_4$ spectrum contains three lines (Fig. 7(c)). It corresponds to a Np(VI) ion in a very deformed polyhedron. Its isomer shift on the plot of $S = f\langle d_{Np-L}\rangle$ (Fig. 1) gives very high Np–O distances, of the order of 2.4 Å, associated with the absence of the neptunyl group. This suggests a coordination which is greater than eight and requires confirmation using other methods.

$K_2Np_2O_7$ shows a spectrum of the same kind; the higher S value indicates the presence of an NpVI ion in VII coordination, in a very distorted site. The values of the hyperfine parameters exclude the existence of the NpO_2^{2+} ion in these two compounds.

The Mössbauer spectrum for $Na_2Np_2O_7$ reveals a more complex environment. The best results are obtained by allowing three different sites for Np(VI): (a) flattened octahedron with a vacancy in the neptunyl group; (b) seven coordinated neptunium in a very distorted site; (c) a very symmetrical site, with the neptunium ion seven coordinated.

The hyperfine parameters of these compounds are shown in Table 2.

3.2. Neptunium(III) compounds

The oxidation state III of neptunium is unstable. The only trivalent compounds synthesized are simple halides, chalcogenides or pnictides. The Np(III) ion may be stabilized in a very ionic environment: the ternary fluorides of the BaF_2-NpF_3 system [44] which has been studied by X-ray diffraction and Mössbauer spectrometry. The corresponding uranium systems, although

TABLE 2

Mössbauer parameters for hexavalent neptunium compounds at 77 K

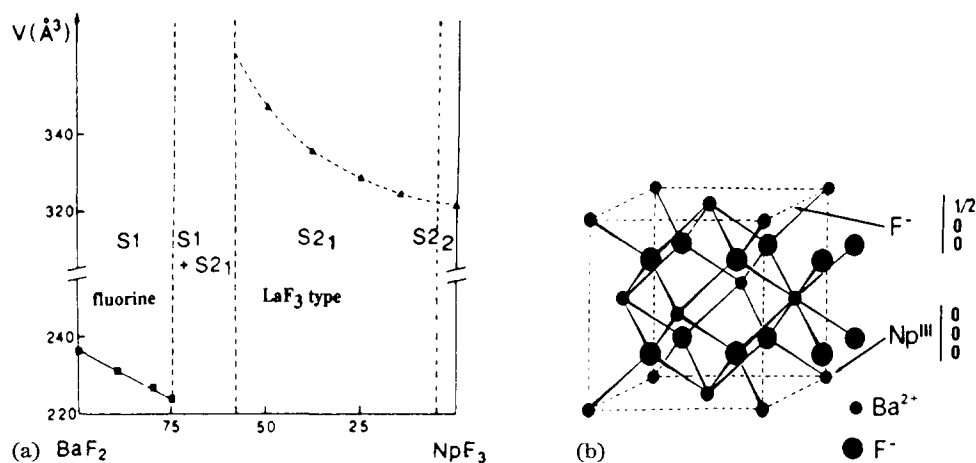| Compound		$S/NpAl_2$ (mm s^{-1})	e^2qQ (mm s^{-1})	η
$K_9Np_6O_{22.5}$		$-56.1(5)$	$96.6(5.0)$	0.00
$Na_2Np_2O_7$	Site A	$-53.7(5)$	$166.0(1.0)$	$0.51(5)$
	Site B	$-48.6(5)$	$83.0(2.0)$	$0.80(6)$
	Site C	$-46.3(5)$	0.00	
$K_2Np_2O_7$		$-51.2(5)$	$119.5(1.0)$	1.00
$CaNpO_4$		$-31.9(5)$	$90.6(1.0)$	1.00

Fig. 8. Solid solution in the BaF_2–NpF_3 system. (a) Variation of the cell volume $vs.$ concentration of BaF_2: S1 = fluorine type; S2$_1$ = hexagonal, LaF_3 type; S2$_2$ = rare earth type. (b) S1 fluorine cell, F$^-$ anions have an interstitial position in the lattices.

widely studied, are poorly understood. With neptunium, two solid solutions have been revealed, as shown in Fig. 8(a).

3.2.1. The Si area, fluorine type (Fig. 8(a))

The Mössbauer spectrum contains a single line (Fig. 9(c)), which is characteristic of Np(III) ($S = +40$ mm s^{-1} [1]). Table 3 shows that S remains invariable for the different compositions studied, and $e^2qQ = 0$ indicates an environment of cubic symmetry at the Np(III) site. As in rare earths, a Ba^{2+} cation is replaced by a Np(III) cation and an F$^-$ anion comes into an interstitial position (Fig. 8(b)), in order to preserve charge equilibrium. The stoichiometry of this solid solution is:
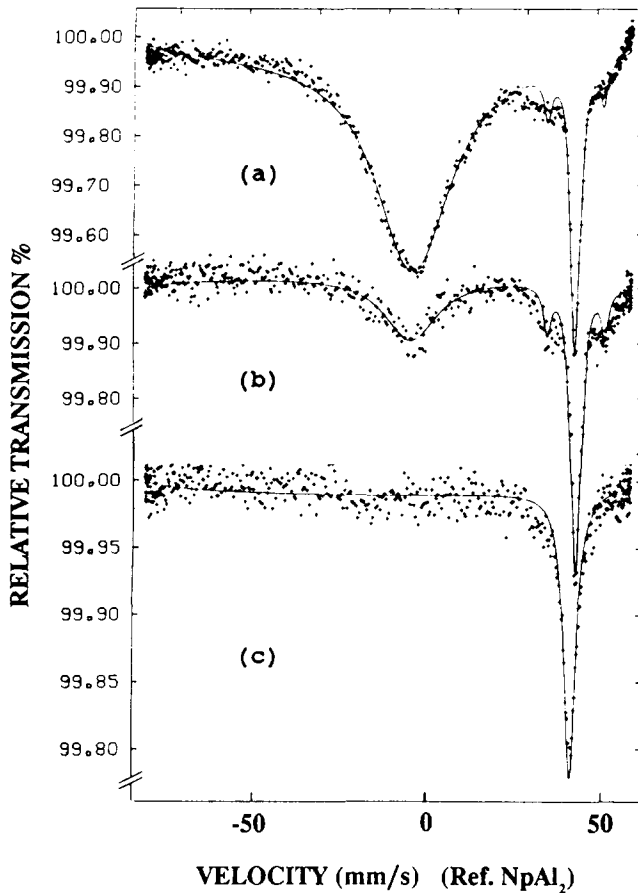
$$Ba_{1-x}Np_x^{III}F_{2+x} \qquad 0 < x < 0.25.$$
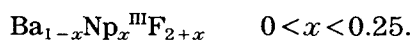
Fig. 9. Mössbauer spectra at 4.2 K. (a) $Ba_{0.5}Np^{IV}_{0.45}Np^{III}_{0.05}F_{2.95}$, (b) $Ba_{0.334}Np^{IV}_{0.283}Np^{III}_{0.383}F_{2.95}$, (c) $Ba_{0.8}Np^{III}_{0.2}F_{2.2}$.

3.2.2. Type LaF₃, S2 area (Fig. 8(a))

Mössbauer spectrometry reveals the presence of two neptunium charge states, III and IV (Fig. 9(a), (b)). The values of the Mössbauer parameters are given in Table 3. In order to interpret these results, it is necessary to have recourse to a new substitution mechanism: Np(III) being substituted to Ba^{2+} and Np(IV) with the creation of vacancies, leading to $Ba_{y+x}Np^{III}_{1-y-2x}Np^{IV}_xF_{3-y}\blacksquare_y$ ($S2_1$).

The study by Mössbauer spectra of variation of the ratio in the areas corresponding to the two neptunium sites allows the experimental determination of y; it is found to be equal to 0.05. The composition limit is reached when all the Np(III) has been substituted: $Ba_{0.05}Np^{III}_{0.95-2x}Np^{IV}_xF_{2.95}\blacksquare_{0.05}$ (charge neutrality). By analogy with rare earths and from measurements performed on the NpF_3–ZrF_4 system it was concluded that a $Ba_yNp^{III}_{1-y}F_{3-y}\blacksquare_y$-type solution should exist for $y < 0.05$ ($S2_2$).

TABLE 3

Mössbauer parameters for the solid solution BaF_2–NpF_3

	Composition	Np(III)			Np(IV)	
		S (mm s^{-1})	e^2qQ (mm s^{-1})	η	S (mm s^{-1})	Np^{IV} (mol%)
S1	$Ba_{0.8}Np^{III}_{0.2}F_{2.2}$	38.9(0.6)	0			
	$Ba_{0.75}Np^{IV}_{0.09}Np^{III}_{0.16}F_{2.34}$	39.2(0.6)	0		−6.0(0.6)	36.4(1.0)
S2	$Ba_{0.5}Np^{IV}_{0.45}Np^{III}_{0.05}F_{2.95}$	40.1(0.6)	27.0(3)	1	−6.1(0.6)	86.5(2.0)
	$Ba_{0.334}Np^{IV}_{0.283}Np^{III}_{0.383}F_{2.95}$	40.3(0.6)	27.7(3)	1	−5.9(0.6)	45.1(1.0)
	$Ba_{0.25}Np^{IV}_{0.2}Np^{III}_{0.55}F_{2.95}$	40.1(0.6)	28.0(3)	1	−5.9(0.6)	27.3(1.0)
	$Ba_{0.15}Np^{IV}_{0.1}Np^{III}_{0.75}F_{2.95}$	40.1(0.6)	36.0(3)	1	−6.1(0.6)	11.5(0.5)
	NpF_3	39.6(0.6)	16.0(2)	1		

The mole percentage is determined by the ratio of the area of the Np^{IV} and Np^{III} spectra.

3.3. Neptunium(IV) compounds
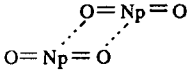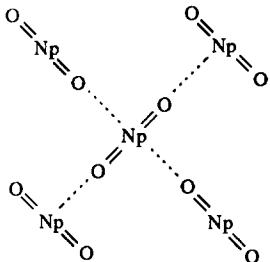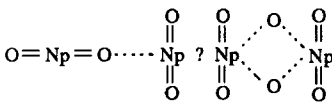
Remarkable results can be noted for the perovskite-type compound $BaNpO_3$ [19, 24]. The neptunium octahedron environment, imposed by the perovskite structure (Fig. 3(a)), which is unusual for an Np(IV) ion, gives rise to a particular behaviour. Shorter distances in $BaNpO_3$ (CN=VI, $\langle d_{Np-L}\rangle = 2.3$ Å) than in NpO_2 correspond to a more negative S value (-10.3 mm s^{-1} [5] instead of -6.1 mm s^{-1}). It should be noted that this value is even more negative than that measured for the fluoride $CoNpF_6 \cdot xH_2O$, for which $S = -6.7$ mm s^{-1}. The quadrupolar splitting value of 14 mm s^{-1} for $BaNpO_3$ indicates a distortion of the octahedron. Although $BaNpO_3$ is located at the limit of the area of the pentavalent compounds on the isomer shift scale, its charge state is clearly IV. It will be seen that the perovskites are the most ionic neptunium oxides. For the Np(V) ion in an octahedron, the S value is close to -30 mm s^{-1}.

3.4. Neptunium(V) compounds

The study of a single crystal of Na and Np(V) mellitate: $Na_4(NpO_2)_2C_{12}O_{12} \cdot 8H_2O$ [22] has revealed the existence of the $(NpO_2^+)_2$ dimer (Table 4), with two neptunium atoms closely related, $d_{Np-Np} = 3.48$ Å; the neptunyl groups surrounded by four mellitic anions form a bidimensional arrangement. In $(NpO_2)_2SO_4 \cdot 2H_2O$, the flattened pentagonal bipyramids surrounding the Np(V) ion are connected by the oxygen atoms from neptunyl groups (as shown in Table 3) [23]. The Np–Np distances are between 4.08 and 4.2 Å, excluding metal–metal bonding; NpO_2^+ groups are isolated entities. An analogous structure is revealed in the Np(V) pyromellitate [47]. Table 4 shows that the Mössbauer parameters, e^2qQ and B_{eff} are very similar for these two compounds. The existence of metal–metal bonding in $Na_4(NpO_2)_2C_{12}O_{12} \cdot 8H_2O$ should strongly affect the values of S and e^2qQ. The similarity of the hyperfine parameters in the two compounds (dimer and

TABLE 4

Comparison of the Mössbauer parameters at 4.2 K, for Np^V frozen solutions and polycrystalline compounds

Compounds	$S/NpAl_2$ (mm s⁻¹)	e^2qQ (mm s⁻¹)	B_{eff} (kOe)	Species
$Na_4(NpO_2)_2C_{12}O_{12}$, H_2O Polycrystalline sample	−20.4 (0.5)	94 (1.0)	5270 (50)	$O{=}Np{=}O$ / $O{=}Np{=}O$
$(NpO_2)_2SO_4$, $2H_2O$ Polycrystalline sample	−17.7 (0.5)	82.4 (1.0)	4910 (50)	(bridged Np–O network structure)
Frozen solution Np(V) = 0.1 M HClO₄ = 1 M Monomer	−17.2 (0.5)	103.2 (1.0)	5119 (50)	$O{=}Np{=}O$
Np(V) = 0.5 M HClO₄ = 1 M Dimer NaClO₄ = 5 M	−17.2 (0.5)	105.6 (1.0)	4999 (50)	$O{=}Np{=}O \cdots Np\ ?\ Np$ (dimer)

Value for magnetic splitting: 1 mm s⁻¹ = 0.05018 × 10⁶ G, assuming $\mu_g = 2.5$ nm for ^{237}Np.

monomer) implies the same local order around the neptunium and the absence of such a bonding.

Guillaume *et al.* [46] have shown the existence of the Np(V)–Np(V) dimer in concentrated solutions of Np(V) in an acidic medium. These cation–cation complexes exist in solution between An^V and M^{III}, M = Cr, Sc, Ga, Fe and Rh, between An^V–An^V and between An^V–An^{VI}. The structure of the first hydration sphere is not well known.

Frozen solutions of Np^V have been studied using Mössbauer spectrometry. A local order is set up when a solution is rapidly cooled. The frozen solution should have the structure of glass or of a microcrystal, with a short-range order. The Mössbauer spectra of $Np^V = 0.1$ M (monomer) and $Np^V = 0.5$ M (dimer) (Fig. 10) solutions (Table 4), collected at 4.2 K, are identical, and are the same as those obtained for $Na_4(NpO_2)_2C_{12}O_{12} \cdot 8H_2O$ and $(NpO_2)_2SO_4 \cdot 2H_2O$, studied in the form of crystalline powders. The hyperfine parameters of these compounds and in the frozen solution are very similar. Their coordination polyhedra must be the flattened pentagonal bipyramid containing the neptunyl group for all them. The spectra of the frozen solutions are altered by paramagnetic relaxation phenomena ($T_r \gg 6.8 \times 10^{-8}$ s) for the two spectra studied, and the lines are broadened (8 mm s⁻¹). The
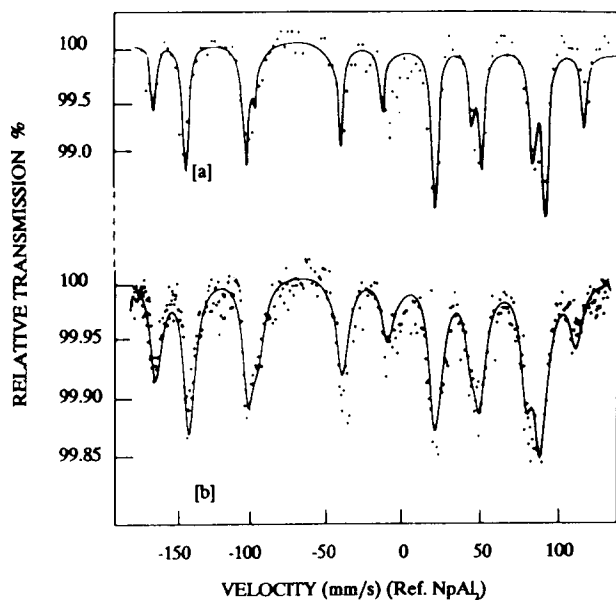
Fig. 10. Mössbauer spectra at 4.2 K of: (a) $Na_4(NpO_2)_2C_{12}O_{12} \cdot 8H_2O$; (b) $Np^V = 0.5$ M frozen solution, $HClO_4 = 1$ M, $NaClO_4 = 5$ M.

positions of the lines are, however, correctly adjusted [48]. In the acidic solutions of Np(V), two forms of the dimer have been proposed (Table 4) which are different from those observed in the solid state; only one of the actinyl ions is affected and the NpO_2^{2+} ions are "bridged" by ligands. A slight difference in the values of the parameters of $Na_4(NpO_2)_2C_{12}O_{12} \cdot 8H_2O$ which contains the dimer is noted. The results regarding Np^V are still insufficient to permit a correct interpretation.

3.5. Neptunium(VII) compounds

The heptavalent neptunium compounds have been widely studied [36, 50, 51], but in the absence of structural information it has not been possible to link Mössbauer parameters to structure. Two series of single crystals were studied, but the quantities were too small to allow Mössbauer measurements. Very ionic compounds of heptavalent neptunium have been investigated: Ba_2LiNpO_6 and Ba_2NaNpO_6 of the perovskite type [52] and Na_5NpO_6 and K_3NpO_5. In the favourable case of the perovskites it has been possible to correlate isomer shift to structure.

In these perovskites, the Np^{VII} (NpO_6^{5-}) ion is at the centre of a regular octahedron, as shown by the absence of quadrupole splitting ($e^2qQ = 0$), Mössbauer spectrum identical to that of Ba_2ZnNpO_6 in Fig. 4(a)). This allows the determination of Np–O distances: $d_{Np-O} = 2.05$ Å. An increase of S with coordination should be expected. The value of S (-78.8 mm s^{-1}) measured for Ba_2NaNpO_6, is the most negative observed for a neptunium compound and must therefore correspond to the minimal coordination of Np^{VII}. However, a structural study on a polycrystalline sample of $KNpO_4$ conducted by Grigor'ev

et al. [12] revealed that for the less negative S value (-65.1 mm s^{-1} for KNpO$_4$), there was still an octahedron around Np(VII). It may thus be anticipated that for all Np^{VII} compounds, neptunium is at the centre of an octahedron, which may or may not be deformed, depending on the value of e^2qQ.

The Mössbauer spectrum of a frozen solution of Np(VII) $= 7 \times 10^{-2}$ M in a 2.5 M solution of LiOH is the same as that of the crystallized compound: LiNpO$_4 \cdot 2$H$_2$O (same S and e^2qQ values) [49].

It may thus be concluded that the Np(VII) environment is the same in the frozen solution and in the crystallized compound. The e^2qQ value, which is lower than that of KNpO$_4$, does not allow us to conclude the presence of the neptunyl group. Recently, Appelman *et al.* [53] studied solutions of Np(VII) at ambient temperature (273–315 K) using nuclear magnetic resonance and proposed the occurrence of NpO$_4$(OH)$_2{}^{3-}$, entities in solution. This corresponds to an elongated octahedron, in agreement with the hexacoordination observed in the solid state.

4. Comparison of X-ray absorption measurements at the L$_{III}$ threshold and of Mössbauer isomer shift in neptunium compounds

Ionocovalent neptunium compounds at various charge states (III–VII) were studied by X-ray absorption near-edge structure at the Np–L$_{III}$ threshold [54, 55]. The fine structure of the thresholds can be interpreted in terms of the electronic structure. The intense resonance of the L$_{III}$ thresholds has a bearing on the empty electronic states of f symmetry.

A single peak for trivalent and tetravalent neptunium compounds, and a line with a shoulder which can be deconvoluted into two peaks for the Np(V), Np(VI) and Np(VII) compounds are observed. With an increasing of valence state from (III) (NpI$_3$) to (VII) (CsNpO$_4$) the centre of gravity of these white lines (W$_L$) structures shift to higher energy.

The differences observed in the W$_L$ positions, ΔE(L$_{III}$) are interpreted in terms of differences in Coulomb energies of the 2p$_{3/2}$ core-excited neptunium atom with an extra 6d electron. In eqn. (1), ΔU_{cf} and ΔU_{cd} represent the difference in Coulomb attraction between the 2p$_{3/2}$ core hole and the 5f(6d) electron; the ΔU_{fd} term derives from the interelectronic repulsion of 5f and the excited (6d) electron.

$$\Delta E(\text{III}) = \Delta U_{cf} + \Delta U_{cd} - \Delta U_{fd} \tag{1}$$

The theoretical value calculated for ΔE(L$_{III}$) $= 4.8$ eV between Np(III) (5f^4) and Np(IV) (5f^3) in agreement with the measured value of 4.0 eV between NpO$_2$ and NpI$_3$.

The double peaks observed for the higher charge states is interpreted in terms of core-ionized final states with different 5f occupancies.

Neptunium makes it possible to compare the results of the high-energy probe (L$_{III}$ edge X-ray absorption) with those of the low energy (ground state) Mössbauer spectrometry measurements. A correlation between the shift

of the centre of gravity of the L_{III} peak and the Mössbauer isomer shift has been observed in a series of ionocovalent compounds (Fig. 11). The comparison with the isomer shift scale in Table 1 shows remarkable similarities: distribution of the compounds according to clearly defined areas corresponding to the various oxidation states, with maximal effects for Np(III) and Np(IV). This curve varies in a manner analogous to that obtained by plotting S as a function of the $\rho_e(0)$ calculated values. The values measured for Np(VII) differ considerably from those obtained by extrapolation of those corresponding to Np(III) and Np(IV).

The empirical relationships (eqns. (2) and (3)) permit a comparison of $E(L_{III})$ and S:

$$E(L_{III}) = E_0 - a_L(n_{5f}) - b_L(n_{6d}) \tag{2}$$

$$S = S_0 + a_d(n_{5f}) + b_d(n_{6d}) - c_d(n_{7s}) \tag{3}$$

where a_L, b_L, a_d, b_d and c_d are functions of the occupancies of 5f, 6d and 7s states.

The increase of n_{5f} and, to a lesser extent, n_{6d} produces a decrease in $E(L_{III})$ and, in relation to the screening effect, a decrease in the density of the s electrons in the nucleus, and consequently an increase in S.
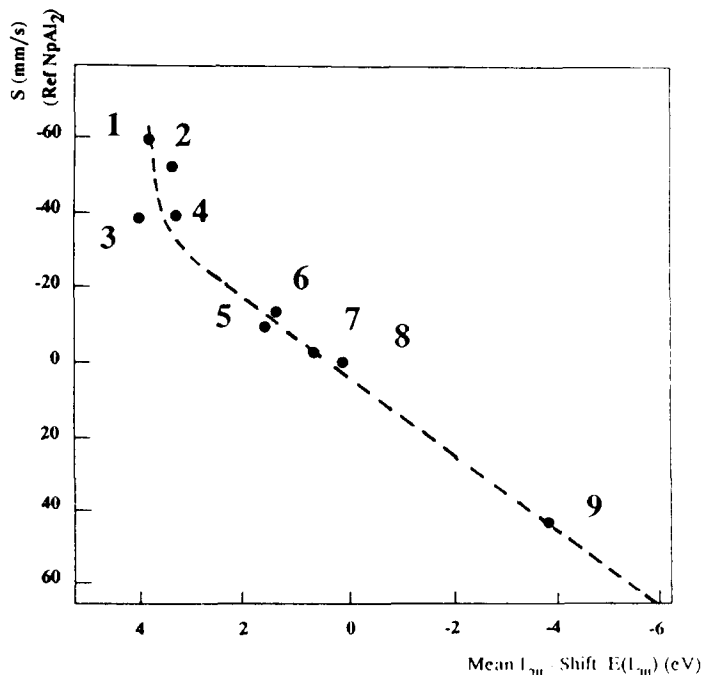

Fig. 11. Isomer shift *vs.* mean L_{III} shift $E(L_{III})$(eV) for neptunium salts. $1 = CsNp^{VII}O_4$, $2 = Ba_2CoNp^{VI}O_6$, $3 = K_2(Np^{VI}O_2)_2V_2O_8$, $4 = NaNp_2^{VI}O_7$, $5 = NH_4Np^VO_2F_2$, $6 = Na_4(Np^VO_2)_2$-$C_{12}O_{12} \cdot 8H_2O$, $7 = BaNp^{IV}O_3$, $8 = Np^{IV}O_2$, $9 = Np^{III}I_3$.

These two methods are very suitable for the study of the occupancy of the 5f orbitals, the localization of the 5f electrons and the covalency effects of the actinide compounds.

5. Relationship between the electronic structure, isomer shift and the electrical field gradient

Many possible contributions participate in the bonding of the early actinide compounds (Th–Am): the diffuse, weakly bound, "fluffy" 7s and 7p that are relatively unimportant, the 6d and 5f that do most of the covalent bonding, and the semicore 6p, whose full importance has been realized only recently [31, 32].

Here we investigate penta- hexa- and heptavalent neptunium compounds with Np–O and Np–X bonds, ranging from the multiple in (NpO_2^{n+}) to the single in the series ($NpO_2^+)O_5^{9-}$, NpO_4^{2-}, NpO_6^{6-}, NpO_6^{8-}, NpO_8^{10-}, NpF_6 and NpO_6^{5-}. The interpretation of the ^{237}Np quadrupole coupling constants, as well as the isomer shift values obtained from the Mössbauer spectroscopy [19] are given at a semiempirical level.

In order to discuss the possible explanations for the observed trends, one of us [56, 57] has carried out calculations using the relativistic extended Hückel REX method. If our results are compared with literature data, it is seen that calculated 5f and 6d populations obtained by Ellis et $al.$ [58] are significantly higher than ours, while the 6p populations are comparable.

For K_2NpO_4, the following Mulliken populations were calculated: $7s^{0.005}$, $6p^{5.69}$, $6d^{0.29}$, $5f^{2.58}$. This result shows the absence of 7s electrons, a considerable 5f (2.58) electron participation, a value which must be compared with $5f^1$ free-ion configuration, and a 6p electron contribution to the bonding.

The calculated Mulliken atomic orbital populations may be correlated to the isomer shift (Fig. 12). For the 5f population in Np^V, Np^{VI} and Np^{VII} oxides, this line is parallel to that obtained for the theoretical values calculated for free neptunium ions. For NpF_6, the $5f^{1.6}$ calculated Mulliken population falls near the ionic line. The plot for the fluorides NpF_x, $x = 3–6$, $vs.$ calculated electronic nuclear density (assuming pure ionic configurations) shows a deviation from linearity [4]. This deviation is attributed to covalency effects [4], increasing when going to higher charge state. The high covalency character of the bonding in Np^{VI} and Np^{VII} compounds may be connected to the overlapping populations, mainly because of the neptunyl group as shown in Table 5. In hexavalent neptunium compounds, the presence of the neptunyl group NpO_2^{2+} in K_2NpO_4 induces a higher overlap compared with Ba_2CoNpO_6 regular octahedron; on the contrary, the overlap remains small for the antineptunyl ion in Li_4NpO_5 (Table 5). These overlapping populations increase with the coordination number, $CN = VII$ for $K_3NpO_2F_5$, $CN = VIII$ in NpO_2CO_3 as well as with the isomer shift: the more covalent the bonding, the more positive is the isomer shift. If we compare overlapping populations for
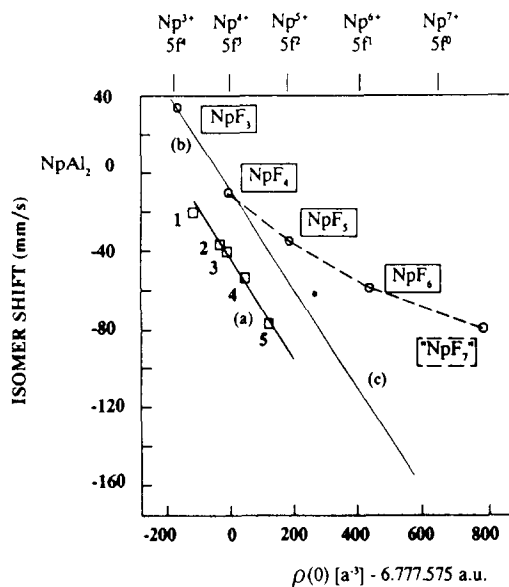
Fig. 12. (a) Experimental isomer shift as a function of the REX 5f Mulliken population for neptunium oxides. $1 = (Np^VO_2)2SO_4 \cdot 2H_2O$, $2 = Np^{VI}O_2CO_3$, $3 = NaNp^{VI}O_2(C_2H_3O_2)_3$, $4 = Ba_2CoNp^{VI}O_6$, $5 = Ba_2NaNp^{VI}O_6$, $* = NpF_6$. See G. M. Kalvius [60]: comparison of the experimental isomer shift of the simple fluorides (b) of neptunium vs. calculated contact densities for the pure $5f^{n+}$ configuration (c).

isomorphic Np(VI) (Ba_2CoNpO_6) and Np(VII) (Ba_2NaNpO_6), perovskite-type compounds, increasing overlapping populations from Np(VI) to Np(VII) correspond to higher covalency in the bonding. This result agrees with the observations of Dunlap and Kalvius [1]. It is possible to explain the general trends of covalency effects but it is not possible to provide a quantitative explanation of the isomer shift.

As shown above, the linear neptunyl group dominates the bonding and induces a strong electric field gradient with the values for hexavalent compounds found in the 95–240 mm s^{-1} range. Until now, the electric field gradient was attributed to two contributions: 5f and 6d electrons and lattice charges. However, recent theoretical studies [59] have suggested that the nuclear quadrupole coupling in actinyl groups would be due to the 6p hole, rather than to the 6d or 5f electrons. In the simplified model where the entire electric field gradient comes from the diagonal term $\langle \frac{3}{2}, \frac{1}{2} \rangle$ a state which corresponds to the $6p_{3/2}$ orbital of neptunium, one finds $q = 4.7 \times 10^{14}$ V cm^{-2} for a one-electron hole in this orbital. The ratio of the observed q with the hole population in the $6p_{3/2}$ orbital gives an estimation of the contribution of the latter to the electric field gradient values, based on the 6p hole. Our calculated electric field gradient values are nearly the same as those which have been measured (Table 6). According to this theory, this would mean that the 6d and 5f participation in electric field gradient, and also the lattice contribution, would be small.

TABLE 5

Mulliken orbital population

Group	Coordination polyhedron	d_{Np-L} (Å)	Mulliken's populations 7s	6p	6d	5f	6p hole	Overlap[a] populations	Charge[b] Np	Ligand
$(NpO_2^{4+}O_2)^{6-}$ Li$_4$NpO$_5$		1.984×4	0.006	5.74	0.22	2.42	–	0.121×4	4.69	-1.65×4 O$_2$
$(NpO_2^{2+}O_4)^{6-}$ K$_2$NpO$_4$		1.89×2 2.16×4	0.005	5.69	0.29	2.58	0.119	0.236×2 0.024×4	4.43	-1.47×2 O$_1$ -1.87×4 O$_2$
NpF$_6$		1.976×6 1.976×6[c]	-0.013 0.070	5.85 5.98	0.10 1.54	1.64 3.85	–	-0.043×6	5.41	-0.90×6 F$_2$
$(NpO_2^{2+}O_5)^{8-}$ K$_3$NpO$_2$F$_5$		1.75×2 2.23×5	-0.008	5.52	0.20	2.82	0.249	0.418×2 0.029×5	4.46	-1.28×2 O$_1$ -0.98×5 F$_2$
$(NpO_2^{2+}O_6)^{10-}$ NpO$_2$CO$_3$		1.67×2 2.48×2 2.52×4	-0.011	5.42	0.27	3.07	0.311	0.520×2 0.015×6	4.23	-1.10×2 O$_1$ -1.97×6 O$_2$

Mulliken orbital population is defined as: $P_a = P_{aa} + \sum_{a \neq b} P_{ab}$ where $P_{i,aa}^{occ} = \sum_i^{occ} c_{ia}^2$ and $P_{ab} = \sum c_{ia} c_{ib} S_{ab}$ with $S_{ab} = \{\Phi_a | \Phi_b\}$, Φ_a and Φ_b being the atomic orbitals utilized and c_{ia}, c_{ib} their coefficients in the Mulliken orbital expansion. There, the P_{aa} are the net orbital populations and the P_{ab} are the overlap orbital populations.

[a] Atomic overlap populations.
[b] Atomic charge.
[c] See ref. 58.

TABLE 6

Electric field gradient values

Compound	$S/\text{NpAl}_2{}^a$ (mm s^{-1})	CN^b	6p hole $6p_{3/2}$ ($m=\frac{1}{2}$)	$eq_{\text{calc}}{}^c$ (10^{18} V cm^{-2})	$eq_{\text{exp}}{}^d$ (10^{18} V cm^{-2})	Overlap^e Np–O
$(\text{Np}^V\text{O}_2)\text{SO}_4$	-18	$2+5$	0.16	6.5	4.4	0.31 O$_1$
$\text{Ba}_2\text{CoNp}^{VI}\text{O}_6$	-59.3	6	–	–	–	0.20 O$_2$
$\text{K}_2\text{Np}^{VI}\text{O}_4$	-56.9	$2+4$	0.11	5.12	4.4	0.28 O$_1$
$\text{K}_3\text{Np}^{VI}\text{O}_2\text{F}_5$	-52	$2+5$	0.25	11.7	9.8	0.35 O$_1$
$\text{Np}^{VI}\text{O}_2\text{CO}_3$	-35.6	$2+6$	0.31	12.9	11.2	0.54 O$_1$
$\text{Ba}_2\text{LiNp}^{VII}\text{O}_6$	-78	6	–	–	–	0.38 O$_2$

^{a}Isomer shift relative to NpAl$_2$.
^{b}CN: coordination number of the neptunium ion.
^{c}Calculated 6p hole contribution.
^{d}Experimental values of the electric field gradient from Mössbauer spectroscopy.
^{e}Overlap population between neptunium and oxygen first neighbours.

6. Outlook for further work

The following research studies would help to fill the gap in current knowledge.

(1) Studies on the pentavalent neptunium compounds for which only poor information exists;

(2) structural studies on single crystals of heptavalent neptunium and EXAFS measurements in order to correlate Mössbauer parameters and local environment in these compounds;

(3) studies of amorphous compounds, glass, frozen solutions and compounds with vacancies in which relaxation phenomena play a predominant role;

(4) further theoretical calculations on insulating compounds in order to interpret isomer shift and electric field gradient in terms of electronic structure.

References

1 B. D. Dunlap and G. M. Kalvius, in A. J. Freeman and G. H. Lander (eds.), *Handbook on the Physics and Chemistry of the Actinides*, Vol. 2, North-Holland, Amsterdam, 1985, Chap. 5.
2 B. D. Dunlap and G. M. Kalvius, in G. K. Shenoy and F. E. Wagner (eds.), *Mössbauer Isomer Shifts*, North-Holland, Amsterdam, 1978, Chaps. 2 and 11.

3 J. A. Stone and W. L. Pillinger, *The Mössbauer Effect, Symp. Faraday Soc.*, Vol. 1, Butterworth, London, 1968, p. 77.

4 G. M. Kalvius, *J. Nucl. Mater.*, *166* (1989) 5.

5 D. G. Karraker, *Adv. Chem. Ser.*, *194* (1981) 347.

6 G. Adrian, *Inorg. Chim. Acta*, *139* (1987) 323.

7 J. G. Stevens and W. L. Gettys, Isomer shift reference scales, *Int. Conf. on the Application of the Mössbauer Effect, Jaipur, India, 1981*, University of North Carolina, Asheville, NC, p. 404.

8 L. He, J. Jové, J. Proust and M. Pagès, *19èmes Journées des Actinides, Madonna di Campiglio, Italy, 1989*, to be published.

9 J. M. Friedt, G. K. Shenoy and M. Pagès, *J. Phys. Chem. Solids*, *39* (1978) 1313.

10 L. He, J. Jové, J. Proust, M. Pagès, C. Madic, J. Litterst and J. Gal, *19èmes Journées des Actinides, Madonna di Campiglio, Italy, 1989*, unpublished.

11 M. S. Grigor'ev and A. V. Ananév, *Prikl. Yad. Spectrosk.*, *12* (1983) 230.

12 M. S. Grigor'ev, M. P. Glazunov, M. P. Mefeod'eva, N. N. Krot, E. F. Makarov, Yu. V. Permyakov and B. G. Zemskov, *Radiokhymia*, *21* (1979) 659 (Engl. Transl. *21* (1980) 572).

13 (a) B. D. Dunlap, G. K. Shenoy, G. M. Kalvius, D. Cohen and J. B. Mann, in G. Goldring and R. Kalish (eds.), *Hyperfine Interactions in Excited Nuclei*, Gordon and Breach, New York, 1971, p. 709.
(b) G. K. Shenoy and B. D. Dunlap, *Phys. Rev. B*, *13* (1976) 1353.

14 E. Simoni, H. Abazli, A. Cousson and M. Pagès, *Radiochem. Radioanal. Lett.*, *49* (1981) 37.

15 A. Tabuteau and M. Pagès, in A. J. Freeman and C. Keller (eds.), *Handbook on the Physics and Chemistry of the Actinides*, Vol. 3, North-Holland, Amsterdam, 1985, Chap. 4.

16 F. Nectoux, J. Jové, A. Cousson, M. Pagès and J. Gal, *J. Magn. Magn. Mater.*, *24* (1981) 113.

17 M. Bickel, B. Kanellakopulos, H. Appel, H. Haffner and S. Geggus, *J. Less-Common Met.*, *121* (1989) 291.

18 J. Jové, F. Nectoux, A. Tabuteau and M. Pagès, *Int. Conf. on the Applications of the Mössbauer Effect, Proc. Indian Nat. Sci. Acad., Jaipur, India, 1981*, p. 580.

19 J. Jové, A. Cousson, H. Abazli, A. Tabuteau, T. Thevenin and M. Pagès, *Hyperfine Interactions*, *39* (1988) 16.

20 A. Tabuteau, H. X. Yang, J. Jové, T. Thevenin and M. Pagès, *Mater. Res. Bull.*, *20* (1985) 595.

21 T. Thevenin, J. Jové and C. Madic, *J. Less-Common Met.*, *121* (1986) 477.

22 F. Nectoux, H. Abazli, J. Jové, A. Cousson, M. Pagès, M. Gasperin and G. Choppin, *J. Less-Common Met.*, *97* (1984) 1.

23 M. S. Grigor'ev, A. N. Janobcky, A. M. Fedoseev, M. A. Boudantseva, I. T. Grouchkov, N. N. Krot and V. I. Spitsyn, *Dokl. Akad. Nauk SSSR*, *300* (1988) 618.

24 Th. Krüger, *Dissertation*, KFK 3463, Physik Universität, Kernforschung-Zentrum Karlsruhe, F.R.G., 1982.

25 B. D. Dunlap, G. M. Kalvius, S. L. Ruby, M. B. Brodsky and D. Cohen, *Phys. Rev.*, (1968) 171.

26 A. Cousson, H. Abazli, F. Nectoux, J. Jové, M. Pagès and M. Gasperin, *J. Less-Common Met.*, *121* (1986) 405.

27 A. Tabuteau, M. Pagès, J. Livet and C. Musikas, *J. Mater. Sci. Lett.*, *7* (1988) 1315.

28 J. Jové, J. Gal, W. Pötzel, G. M. Kalvius and M. Pagès, *C.R. Acad. Sci. Paris*, *286* (1978) 641.

29 J. P. Desclaux and A. J. Freeman, in G. K. Shenoy and F. E. Wagner (eds.), *Mössbauer Isomer Shifts*, North-Holland, Amsterdam, 1978, Chap. 4, p. 151.

30 J. B. Mann, in G. K. Shenoy and F. E. Wagner (eds.), *Mössbauer Isomer Shifts*, North-Holland, Amsterdam, 1978, Chap. 9.

31 D. E. Ellis, A. Rosén and P. F. Walch, *Int. J. Quantum. Chem. Symp.*, *9* (1975) 351.

32 P. Pyykkö and L. L. Lohr, *J. Inorg. Chem.*, *20* (1981) 1850.

33 G. Ionova and J. Jové, *Radiokhimica*, *3* (1989) 31.

34 J. Jové, A. Cousson and M. Gasperin, *Hyperfine Interactions*, *28* (1986) 853.

35 V. I. Goldanskii and F. F. Makarov, in V. I. Goldanskii and R. M. Mesher (eds.), *Chemical Applications of Mössbauer Spectroscopy*, Academic Press, New York, 1968, p. 102.

36 J. M. Friedt, *Radiochim. Acta*, *32* (1983) 105.

37 L. R. Morss, in N. N. Edelstein (ed.), *Actinides in Perspective, Proc. Actinides 1987, Conference Pacific Grove (38), CA, U.S.A.*, Pergamon, Oxford, 1981.

38 L. R. Morss, C. W. Williams, I. K. Choi, R. Gens and J. Fuger, *J. Chem. Thermodyn.*, *15* (1983) 1093.

39 A. H. Reiss, M. R. Hoekstra, E. Gerbert and S. W. Peterson, *J. Inorg. Nucl. Chem.*, *18* (1976) 148.

40 L. He, A. Cousson, J. Jové, A. Tabuteau, J. Proust and M. Pagès, *18èmes Journées des Actinides, Paris, France, 20–22 April, 1988*, unpublished.

41 M. C. Saine, M. Gasperin, J. Jové and A. Cousson, *J. Less-Common Met.*, *132* (1987) 141.

42 M. Gasperin, A. Cousson, J. Jové and L. He, *J. Less-Common Met.*, *152* (1989) 339.

43 J. Jové, A. Cousson and M. Gasperin, *J. Less-Common Met.*, *199* (1988) 345.

44 H. Abazli, J. Jové and A. Cousson, *J. Less-Common Met.*, *108* (1985) 123.

45 H. Abazli, A. Cousson, J. Jové, M. Pagès and M. Gasperin, *J. Less-Common Met.*, *96* (1984) 23.

46 B. Guillaume, G. M. Begun and R. L. Hahn, *Inorg. Chem.*, *21* (1982) 1159.

47 A. Cousson, *Acta Crystallogr. Sect. C*, *41* (1985) 1758.

48 E. W. Muller, *MÖSFUN, Mössbauer spectra fitting program for universal theories*, Johannes Universität, Mainz, F.R.G., 1980.

49 C. Keller, in A. J. Freeman and C. Keller (eds.), *Handbook of the Physics and Chemistry of the Actinides*, Vol. 3, North-Holland, Amsterdam, 1985, Chap. 3.

50 (a) K. Fröhlich, P. Gütlich and C. Keller, *J. Chem. Soc. Dalton Trans.* (1972) 971.
(b) A. A. Chaikhorskii, *Transl. Radiokhim.*, *17* (1975) 910.

51 A. V. Ananyev, M. S. Grigor'ev and N. N. Krot, *Radiochem. Radioanal. Lett.*, *44* (1980) 217.

52 S. K. Awasthi, L. Martinot, J. Fuger and G. Duyckaerts, *Inorg. Nucl. Chem. Lett.*, *7* (1971) 1945.

53 E. H. Appelman, A. G. Kostka and J. C. Sullivan, *Inorg. Chem.*, *27* (1988) 2002–2005.

54 S. Bertram, G. Kaindl, J. Jové, M. Pagès and J. Gal, *Phys. Rev. Lett.*, *63* (1989) 2680.

55 B. Bertram, G. Kaindl, J. Jové and M. Pagès, *Physica B*, *158* (1988) 1.

56 P. Pyykkö, in S. Wilson (ed.), *Methods in Computational Chemistry*, Vol. 2, Plenum, New York, 1988, p. 136.

57 P. Pyykkö and L. Laaksonen, *J. Phys. Chem.*, *88* (1984) 4892.

58 D. E. Ellis, A. Rosén and V. A. Gubanov, *J. Chem. Phys.*, *77* (1982) 4051.

59 P. Pyykkö, *Inorg. Chim. Acta*, *139* (1987) 243.

60 G. M. Kalvius, *J. Less-Common Met.*, *121* (1986) 353.